Topics in Catalysis
https://doi.org/10.1007/s11244-020-01370-4

ORIGINAL PAPER

Preparation, Characterization and Catalytic Activity in 2-Propanol Conversion of Potassium and Antimony Mixed Oxides

A. Aitlaalim[1] · F. Ouanji[1] · A. Benzaouak[3] · M. Kacimi[1] · M. Ziyad[4] · L. F. Liotta[2]

Abstract

Potassium and antimony mixed oxides were obtained by calcination of the commercial potassium-antimony tartrate trihydrate $K(SbO)C_4H_4O_6.3H_2O$ at temperatures ranging from 300 to 800 °C. The structure varied with temperature as revealed by XRD characterization. The modifications occurring during the calcination process were also studied by FT-IR and DRS spectroscopies, along with by thermal analysis (TG/DTG). The solids were tested in 2-propanol decomposition at 200 °C, used as probe reaction for the investigation of acid-basic and redox properties. The catalytic activity was function of the calcination temperature and the best 2-propanol conversion was achieved with the tartrate precursor calcined at 500 °C that crystallizes forming $KSbO_3$ as main phase along with $K_{0.51}Sb_{2.67}O_{6.26}$ as secondary phase. Under N_2 the activity reached the maximum after 10 min, 80% of 2-propanol conversion was the highest value, over the sample calcined at 500 °C, but rapidly decreased with time on stream and almost declined after 1 h. In the presence of air in the reaction mixture, 85% of 2-propanol conversion was achieved at 200 °C, after 20 min under stream, with the most active sample. By increasing the calcination temperature above 500 °C, the conversion decreased, especially for the sample calcined at 800 °C showing the worse conversion, although the stability over time increased, likely due to the achievement of stable crystalline phases and crystallite sizes. In all cases, the 2-propanone selectivity was close to 100%. This behaviour confirmed the occurrence of a dehydrogenation reaction involving the basic sites typical of KSbxOy oxides along with the redox couple Sb(V)/Sb(III).

Keywords KSbxOy mixed oxides · 2-propanol conversion · Dehydrogenation · 2-propanone formation

1 Introduction

Antimony oxide is widely used in catalysis. It exhibits, in the metallic or oxidized state, excellent catalytic properties. It exists in three phases, such as antimony trioxide (Sb_2O_3), antimony tetroxide (Sb_2O_4) and antimony pentoxide (Sb_2O_5) [1]. The Sb_2O_5 compound does not exist above 525 °C, only Sb_2O_3 and Sb_2O_4 are formed [1]. Sb and their oxides were used as catalysts or promoters in much researches. For instance, antimony oxides are an essential catalyst material, in particular, for selective oxidation of substituted aromatics and the ammoxidation of paraffin to unsaturated acids and corresponding nitriles, as well as the oxidation of alkanes [2]. In addition, one may cite several catalyst formulations such as magnetic nano-$CoFe_2O_4$ supported Sb which demonstrates a high catalytic activity for the one-pot three-component coupling reaction of amines, 1,3-dicarbonyl compounds and nitro-olefin [3]. The TeMO (M = Mo, V and P) catalysts were promoted by Sb for oxidation of isobutene and toluene, in where the activity was explained

✉ M. Kacimi
kacimimohammed@fsr.ac.ma

✉ L. F. Liotta
leonardafrancesca.liotta@cnr.it

1 Faculty of Sciences, Physico-chemistry of Materials and Catalysis Laboratory, Department of Chemistry, Mohammed V University in Rabat, Avenue Ibn Battouta, B.P. 1014, Rabat, Morocco

2 Istituto Per Lo Studio Dei Materiali Nanostrutturati (ISMN)-CNR, via Ugo La Malfa, 153, 90146 Palermo, Italy

3 Laboratory of Spectroscopy, Molecular Modeling, Materials, Nanomaterials, Water and Environment, Environmental Materials Team, ENSET, Mohammed V University in Rabat, B.P. 6207, Avenue des Forces Armées Royales, Rabat, Morocco

4 Hassan II Academy of Sciences and Technology, Km 4, (ex-route de Zair), Avenue Mohammed VI, Rabat, Morocco

Published online: 13 September 2020

by probably entering of antimony into lattice of phase [4, 5]. Tin–antimony oxides catalyst presents a good selectivity to hydrocarbons oxidation when the temperature is relatively higher, related to the segregation of antimony to the surface [6]. On the other hand, referring to the work carried out on Sb modified vanadia on titania, the antimony might reduce the surface acidity [7]. Moreover, antimony oxide promoter of vanadia and ceria displays high performance catalytic dehydrogenation of alkylbenzenes in the presence of CO_2 [8, 9], and on titanium oxide for propane dehydrogenation [10]. Furthermore, the use of Sb-Palygorskite composite showing an exceptional catalytic activity of P-nitrophenol hydrogenation, due to inhibition of nanoparticles aggregation of antimony [11]. The Sb supported zeolite catalyst is more active in conversion of syngas to dimethyl ether [12], and Antimony (1-D) nanostructured porous nanofibers supported Pt was also investigated in oxidation of methanol in DMFCs technology [13]. One can also refer to the work on composite of SnP-(Sb–SnO_2) as active material for oxygen evolution reaction [14]. In addition, the use of antimony as promoters of V_2O_5/TiP shows a high selectivity to phthalic anhydride in oxidation of o-xylene [15]. The V–Sb–O mixed oxide on Al_2O_3, TiO_2 and Nb_2O_5 has been also investigated in selective oxidation of H_2S and propane ammoxidation reaction to acrylonitrile [16–19]. Furthermore, Sb_2O_3 added to silica supported gold nanoparticles leads to high activity in CO conversion [20]. Besides, the addition of antimony to catalyst compounds can give an excellent activity at low-temperature with good sulphur resistance [21]. One quantum chemical study demonstrates that the antimony promoted V_2O_5/TiO_2 is the best catalyst in this sense compared to selenium and copper [22]. It can also improve the catalyst oxidizing property and surface acidity that are beneficial to enhance activity and the selectivity [23].

Udalova et al. have studied the mixed oxide Co–Mo–Bi–Fe–Sb–K catalyst in the partial oxidation of propylene to acrolein. According to their report, the introduction of potassium into the studied phases decrease deep oxidation activity, but even small amounts of these elements raise the selectivity of the catalyst [24]. Indeed, Sb(III) ions can substitute for Bi(III) ions in the bismuth molybdate structure. Being the radius of Sb^{3+} (0.9 Å) smaller than that of Bi^{3+} (1.2 Å), antimony ions distort this structure considerably and this distortion affects the properties of catalysts containing bismuth molybdates. The introduction of equal amounts of K and Sb has the most favourable effect on the selectivity of the catalyst and this effect is likely to be due to the fact that potassium reduces the antimony-induced acidity of the catalyst [24].

The antimony oxides, despite their wide structural varieties, have been rarely tested in the energy production reactions. They have attracted attention in reactions such as the synthesis of polyethylene terephthalate fibers (PET). As a matter of fact, 90% of the world's production of PET has been achieved via antimony based catalysts [25].

Furthermore, antimony was used in photocatalysis. Indeed, S-doped Sb_2O_3 and leaded oxide (PbO) oxide show a good catalytic photodegradation of 4-phenylazophenol and methyl orange under visible-light [26]. Unsupported and supported antimony oxides were also used as catalyst of the esterification of glycerol. In both case their activity and selectivity were correlated to the fact increase of Lewis and Brönsted acidic sites [12, 27]. The amount of the acid sites was also correlated to the Sb loading.

The main goal of the present work is the simple synthesis of mixed oxides of potassium and antimony prepared by decomposition and calcination of potassium and antimony tartrate $K(SbO)C_4H_4O_6.3H_2O$. The resulting catalysts were characterized by different techniques including the evaluation of acid-basic and redox properties by 2-propanol decomposition.

2 Experimental

2.1 Catalyst Preparation

KSbxOy mixed oxides were synthesized as herein reported. Briefly, the precursor, $K(SbO)C_4H_4O_6.3H_2O$ (research grade), was calcined at various temperatures in the range 300–800 °C under air in oven with heating ramp of 10 °C min^{-1}, keeping 2 h at each temperature. The resulting solids were characterized by several techniques, before testing in 2-propanol decomposition, as described below.

2.2 Characterization Methods

The synthesized solids were characterized by XRD at room temperature using a Brucker 5005 diffractometer equipped with copper anode (Kα = 1.54184 Å) and a monochromator. The data were collected with a step size equal to 0.02°, from 2θ = 3°–60°. The crystalline phases were identified by using JCPDC and/or PDF database files and the mean crystallite sizes were determined by Scherrer equation.

Fourier Transform Infrared (FTIR) was used to characterized the changes in precursor structure with the temperature increasing. The spectra have been recorded in transmission mode; using a Jasco 4600 spectrometer with an Attenuated Total Reflection (ATR) module (Pro-One) equipment at a resolution of 4 cm^{-1} and range from 4000 to 400 cm^{-1}.

Specific surface areas (BET method) of the catalysts were acquired from the N_2 adsorption isotherms at – 196° C. The samples were previously treated in situ under vacuum at 200 °C for 2 h. The measurements were performed with a Coulter Omnisorp 100 CX apparatus.

TG/DTA analyses were carried out in order to identify the structural changes occurring in the catalysts after progressive heating. All experiments were performed with a Labsys™ Evo (1F) Setaram instrument under air flow (60 ml min^{-1}) by using 15 mg of sample heating from room temperature up to 800 °C with heating rate of 10 °C min^{-1}.

The UV–Vis–NIR diffuse reflectance spectra were performed on a Varian UV–VIS–NiR spectrophotometer equipped with an integrated sphere over the 200–2400 nm. The spectra were collected at room temperature using PTFE (polytetrafluoroethylene) plate as reference material.

The morphology of the catalyst was studied by Scanning Electron Microscopy (SEM) and Energy Dispersive X-ray spectroscopy (EDX) analyses, using a Jeol JSM-7000F FE-SEM, Japan.

2.3 2-Propanol Conversion

The conversion of 2-propanol was performed at atmospheric pressure and at 200 °C, in a silica fixed bed microreactor. Prior to the tests, the catalyst (100 mg) initially calcined under air at a given temperature (300–800 °C) was treated under nitrogen at 60 mL min^{-1}, at 400 °C for 1 h in order to clean the surface and remove any adsorbed species (except the solid calcined at 300 °C that was pre-treated at 300 °C). Then the reactor was cooled down to the reaction temperature and 2-propanol at a partial pressure of 1.2 kPa was flowed by a saturator fed with N_2 or with air at a total flow rate of 60 mL min^{-1}. The 2-propanol conversion reaction was carried out in isothermal conditions, at 200 °C, versus time, during 90 min. In order to get insights into the catalyst reusability, after performing a first run at 200 °C under N_2 as carrier gas, a regeneration treatment at the same reaction temperature was performed flowing for 1 h air 60 mL min^{-1}, then, after purging 30 min with pure N_2, the reactor was fed with 2-propanol in N_2 for a second run. The reaction products were analysed on-line by using: (i) a ATI Unicam 610 chromatograph with a flame ionization detector equipment and a 4 m packed column with Chromosorb PAW coated by 15% of carbowax 1500 for the 2-propanol, 2-propanone, propene and ether separation, and (ii) a Shimadzu GC-8A equipped with a column of silica gel and TCD detector for analysis of gaseous species, such as CO/CO_2. The reaction features were defined as follows:

$$Conversion = \frac{IPA_{in} - IPA_{out}}{IPA_{in}} \times 100 \quad (1)$$

$$\text{Pr}oduct\ Yield = \frac{Fraction\ of\ IPA\ converted\ to\ product}{IPA_{in}} \times 100 \quad (2)$$

$$\text{Pr}oduct\ Selectity = \frac{\text{Pr}oduct Yield}{Conversion} \times 100 \quad (3)$$

The experimental data of catalytic tests were registered using a PowerChrom 280 data acquisition system.

3 Results and Discussion

3.1 Materials Characterization

3.1.1 XRD Analysis

Figure 1 shows the XRD patterns recorded after calcination of the precursor $K(SbO)C_4H_4O_6.3H_2O$ at different temperatures. The signals of the sample heated at 60 °C belong to the structure of the precursor, suggesting that at this low temperature no decomposition occurs. The sample calcined at 300 °C (Fig. 1b) shows a mixture of two phases, KSb_3O_5 (JCPDC 74–2380) and K_2CO_3 $1.5H_2O$ (PDF #73-0470), while that calcined at 400 °C (Fig. 1c), shows peaks related to KSb_3O_5 (JCPDC 74-2380) [28] along with blending unidentified phases (likely ascribable to organic compounds and carbonaceous species). According to TG/DTA analysis (see Fig. 3), during calcination at 400 °C the sample became initially black due to carbon formation, then turning to white colour after total oxidation of residual species. Based on the crystalline phases detected by XRD, it can be concluded that in the samples calcined at 300 and 400 °C, the Sb valence is mainly + 3. The calcination of the $K(SbO)C_4H_4O_6.3H_2O$ precursor at 500 °C reveals the formation of $KSbO_3$ as preponderant phase along with $K_{0.51}Sb_{2.67}O_{6.26}$ as secondary phase, according to the peaks at 2θ 28.2, 34.2, 49.2 and 51.6° (JCPDS 70-0653) [29]. Such secondary phase disappeared by calcining above 500 °C. Reddy and all [28]. suggested that the formation of K_2O (JCPDC 47-1701) can also

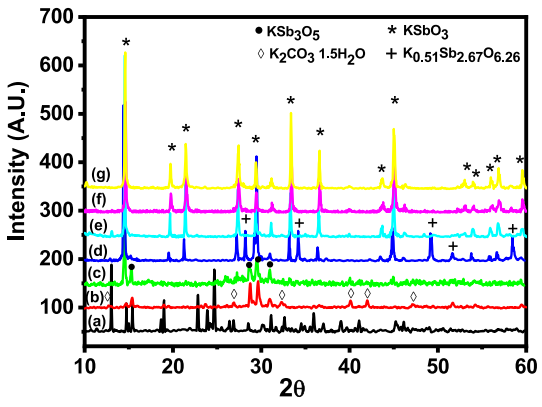

Fig. 1 X-ray diffraction patterns of $K(SbO)C4H_4O_6.3H_2O$, decomposed at different temperatures: 60 °C (a); 300 °C (b); 400 (c); 500 °C (d); 600 °C (e); 700 °C (f); 800 °C (g)

occur at this temperature. However, no signals corresponding to this phase were detected, although we cannot exclude its presence as amorphous phase.

Above 600 °C, all the diffraction patterns (Fig. 1 e-600, f-700 and g-800 °C) match with peaks assigned to the $KSbO_3$ structure (JCPDS 49-0165). Thus, starting from 500 °C, the Sb valence is mainly equal to + 5.

3.1.2 FTIR Spectroscopy

The FT-IR spectra of the $K(SbO)C_4H_4O_6.3H_2O$ calcined at different temperatures are displayed in Fig. 2a, b). In Table 1 the wavenumber and relative peak assignments are listed. The spectrum of the sample treated at 60 °C shows bands located at 3588, 3483 and 3390 cm^{-1} belonging to hydroxyl groups and the adsorbed water. The bands 2888, 2856, 1341, 1305, and 1268 cm^{-1} are assigned to C–H stretching [30]. The stretching of COO− from tartrate appears at 1650 cm^{-1}, while the bands associated with C-O (from CHOH) of the tartaric acid appear at 1130 and at 1074 cm^{-1} [31]. The frequencies at 628, 610, and 540 cm^{-1} characterize the banding

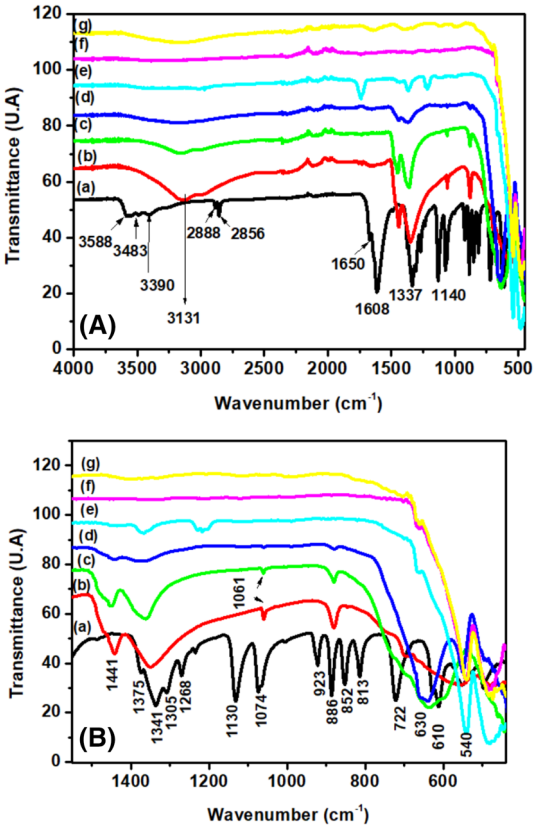

Fig. 2 FT-IR spectra of $K(SbO)C_4H_4O_6.3H_2O$, decomposed at different temperatures: 60 °C (a); 300 °C (b); 400 (c); 500 °C (d). 600 °C (e); 700 °C (f); 800 °C (g). Panel **a** displays the entire range from 4000 to 450 cm^{-1}; in panel **b** the enlarged range 1550–450 cm^{-1} is shown

Table 1 Wavenumber and FT-IR peak assignments

Wavenumber (cm^{-1})	Stretching peak assignments
3588, 3483, 3390	O–H
2888, 2856, 1341,1305, 1268	C–H
1650	COO^-
1130, 1074	C–O
852, 813, 722–3131, 1444, 1375, 1061 878	K–O(KSb and K_2CO_3)
630, 610, 540	Sb–O, O–Sb–O

vibration of (Sb–O) and O–Sb–O bridge functional group of oxide. The FT-IR spectra of the sample calcined above 60 °C show that the intensity of the signals, in the region 2000–450 cm^{-1}, decreases as the calcination temperature increased and the organic matter is decomposed. The spectra also indicate the formation of potassium carbonate between 300 and 400 °C. Their characteristic bands have been observed at 3131, 1441, 1375, 1061 and 878 cm^{-1}, while features at 852, 813, and 722 cm^{-1} are due to K–O stretching [32]. For samples calcined at T ≥ 600 °C only Sb-O stretching bands were detected according with the formation of KSbxOy oxides and total oxidation of the organic precursor.

3.1.3 Specific Surface Area and Crystallite Size by XRD

In Table 2 the specific surface values, calculated by BET method, and the mean crystallite sizes of the main phases, determined by Scherrer equation, are listed for samples calcined at different temperatures. The sample calcined at 300 °C showed the highest specific surface area, equal to 41.7 m^2/g. Then, by increasing the calcination temperature, the specific surfaces decreased up to 11.2 m^2/g, that is the lowest value registered after calcination at 800 °C. At the same time, the crystallite values of the main phases increased from 13 nm, for the phase KSb_3O_5 formed at 300 °C up to 59 nm for the phase $KsbO_3$ after calcination at 800 °C.

3.1.4 Thermal Analyses

In order to obtain supplementary information on the structural change of antimony potassium tartrate ($K(SbO)C_4H_4O_6.3H_2O$), thermo-gravimetric and differential thermal analyses (TG/DTA) were carried out under air flow, as shown in Fig. 3. The mass loss takes place in three main steps. The first one is located between ~ 150 and 250 °C with a broad endothermic peak centred at 185 °C, corresponding to a mass loss of 6% that is associated with the removal of water from the sample. The resulting solid remained stable until 300 °C. Then, at 350 °C a strong modification occurs with a further mass loss, of around 30% at ~ 450 °C, that was

Table 2 Specific surface area values and crystallite sizes of samples calcined at different temperatures

Calcination temperature (°C)	300	400	500	600	700	800
$S_{BET}(m^2 \cdot g^{-1})$	41.7	37.5	24.8	16.1	14.2	11.2
Crystallite size (nm)	13.0 (KSb_3O_5)	18.0 (KSb_3O_5)	23.0 ($KSbO_3$)	37.0 ($KSbO_3$)	45.0 ($KSbO_3$)	59.0 ($KSbO_3$)

In parenthesis the corresponding crystalline phases are reported

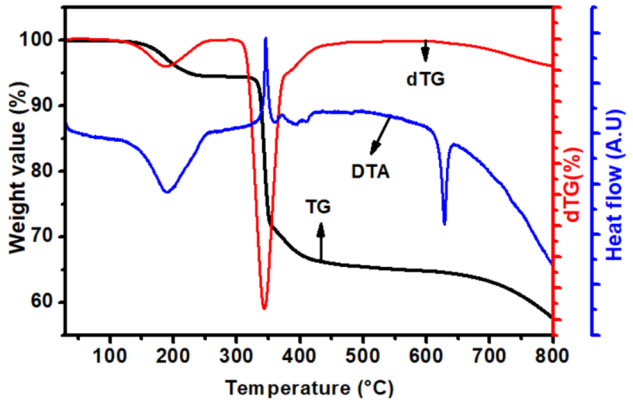

Fig. 3 Thermogravimetric analysis of $K(SbO)C_4H_4O_6.3H_2O$

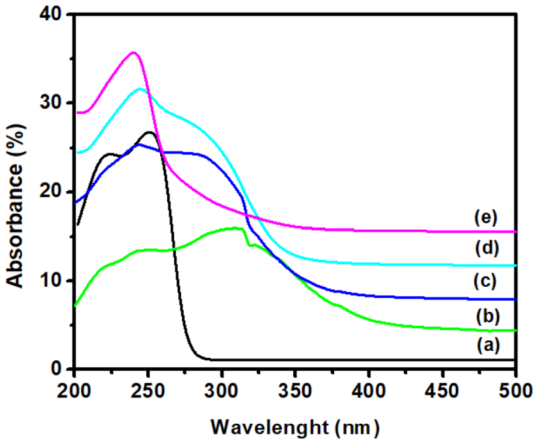

Fig. 4 UV–VIS-PIR DRS of $K(SbO)C_4H_4O_6)\cdot 3H_2O$, treated at: 60 °C (a); 400 °C (b); 500 °C (c); 600 °C (d); 700 °C (e)

attributed to the exothermal oxidation of the tartrate along with of residual carbon species. According with the XRD characterization, at 400 °C a mixed oxide of potassium and Sb(III) antimony, with formula KSb_3O_5, is formed, then at 500 °C $KSbO_3$ as main phase along with $K_{0.51}Sb_{2.67}O_{6.26}$, as secondary phase was detected. By further increasing the temperature, an additional and gradual mass loss is registered from 500 °C to 800 °C up to the final weight value of ~ 57%. Such step is accompanied by a tight endothermic peak at 630 °C likely associated to the crystallization process of the $KSbO_3$ phase.

3.1.5 UV–Visible Spectroscopy (DRS)

The UV–Visible diffuse reflectance spectra of selected samples prepared by decomposition of $K(SbO)C_4H_4O_6.3H_2O$ at different temperatures are displayed in Fig. 4. The parent sample exhibits high optical transparency, reaching almost 80%, with maximum absorption wavelengths below 260 nm (at 251 and 224 nm, respectively). It is worth noting that the electronic band structures of metal oxides are directly related to their constituent elements and their structural arrangement. Moreover, light absorption due to electronic transitions from the valence band (VB) to the conduction band (CB) may occur. In these mixed oxides, the VB and CB are predominantly formed from O 2p and Sb 4d orbitals, respectively [33]. After calcination, the obtained spectra show two large absorption peaks with maximums at around 244 and 314 nm for the material calcined at 400, attributed to the presence of KSb_3O_5. Then, bands at 244, 290 nm and at 244, 286 nm, were detected for the calcined samples at 500 and 600 °C, respectively. Such bands were ascribed to the presence of the $K_{0.51}Sb_{2.67}O_{6.26}$ and $KSbO_3$ crystalline phases. The absorption of the material calcined at 700 °C, corresponding to $KSbO_3$, shifted to the UV range with a maximum peak around 240 nm.

3.1.6 SEM

Figure 5 shows the SEM images of samples calcined at various temperatures. The parent compound treated at 60 °C (Fig. 5a), presents irregular crystallites of different sizes. The sample calcined at 300 °C shows a dense structure (Fig. 5b), turning after calcination at 500 °C and at 800 °C, (Fig. 5c, d respectively) towards an irregular surface constituted by agglomerated flakes and irregular lumps. According with the literature, this morphology is typical of KSb_3O_5, $K_{0.51}Sb_{2.67}O_{6.26}$, and $KSbO_3$ phases [28]. In Table 3 the elemental composition as a function of the calcination temperature is displayed. An evident decrease of the carbon content occurs by increasing the calcination temperatures.

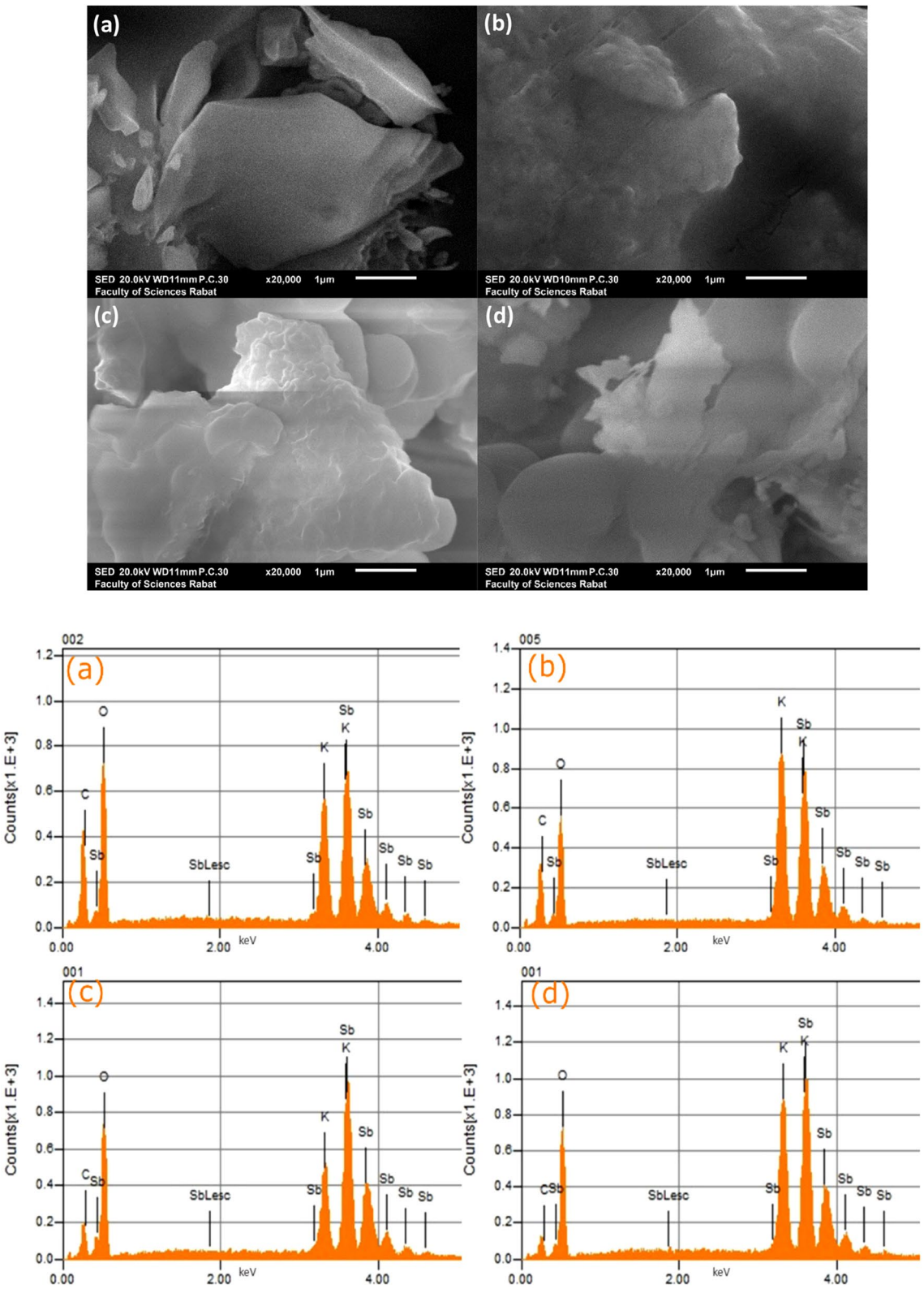

Fig. 5 SEM micrographs and EDS analysis of samples prepared at various temperature 60 °C (**a**), 300 °C (**b**), 500 °C (**c**) and 800 °C(**d**)

Table 3 Chemical composition of the materials treated at various temperatures by EDX analysis

Calcination temperature	60 °C		300 °C		500 °C		800 °C	
Elements	Wt%	Atom%	Wt%	Atom%	Wt%	Atom%	Wt%	Atom%
C	11.24	27.28	8.09	22.01	4.12	14.24	1.68	5.86
O	28.57	52.07	23.77	48.54	20.11	52.17	20.93	54.91
K	12.31	9.18	19.68	16.44	10.78	11.44	17.21	18.48
Sb	47.87	11.46	48.45	13	64.99	22.16	60.18	20.75
Total	100	100	100	100	100	100	100	100

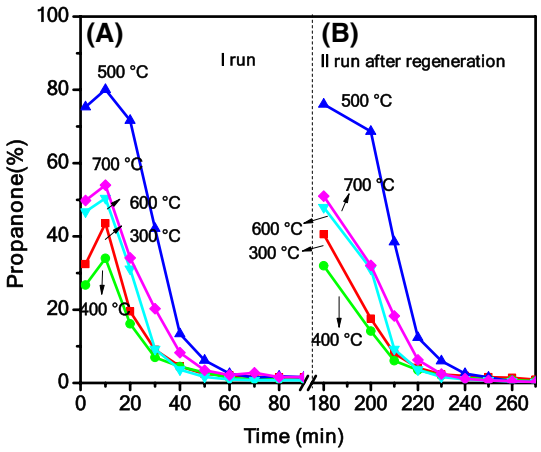

Fig. 6 **a** (I run) Catalytic activity at 200 °C versus time on stream, in the presence of N_2 as carrier gas, for catalysts at different calcination temperatures; **b** II run performed in the same condition after regeneration at 200 °C 1 h under air flow

4 2-Propanol Conversion

In order to investigate the acid-basic and redox properties of the catalysts calcined at different temperatures, the 2-propanol decomposition reaction was carried out using a mixture of the alcohol (at a partial pressure equal to 1.27 kPa) diluted in N_2 or air. It is generally accepted that dehydration to propene occurs on acidic sites, whereas the base and/or redox sites are responsible for dehydrogenation to 2-propanone [34, 35]. Considering that the selective alcohols oxidation to ketones and aldehydes is a key technology in the chemical industry, providing important intermediates for pharmaceuticals and fine chemicals [36], we have considered worthy of investigation the 2-propanol conversion, as probe reaction for the assessment of the acid-basic properties of the catalyst [37].

4.1 Catalytic Activity Under N_2

Figure 6, panel (A) displays the catalytic activity, in terms of propanone formation (%) versus time on stream (90 min) registered at 200 °C, in the presence of N_2 as carrier gas, for samples calcined at different temperatures. 2-propanone was the main product formed by the dehydrogenation of 2-propanol. The activity of the samples, depending on the calcination temperature, was quite high in the first minutes of the reaction, reaching the maximum after 10 min, but rapidly decreased with time on stream and almost declined after 1 h. 80% of 2-propanol conversion was the highest value achieved with the sample calcined at 500 °C. It is likely that in absence of any oxygen coming from the gas phase, the Sb (III) species formed by reaction with 2-propanol cannot be re-oxidized to the pristine Sb (V) sites, therefore, further adsorption of the 2-propanol on the surface of the catalysts blocks the basic sites, poisoning the surface of the catalyst [38]. In order to confirm such hypothesis, after the first catalytic run (Fig. 6a), the catalysts were regenerated at 200 °C for 1 h flowing air 60 mL min^{-1}, during such step CO_2 evolution was registered. Then, after purging 30 min with pure N_2, the reactor was fed with 2-propanol in N_2 for a second run. As it is shown in Fig. 6, panel (B), the catalyst almost regains its initial activity suggesting that the deactivation was due to the poisoning of the active sites by deposition of unreacted C_xH_y species or due to the reduction of all Sb(V) active sites to Sb(III) by 2-propanol. In all cases, the 2-propanone selectivity was close to 100% during all the reaction time, even when after high activity during in the first minutes of the reaction, all the Sb (V) sites are reduced to Sb (III). Such finding confirms that the strong basic sites typical of KSbxOy oxides [39] also contributed to the dehydrogenation reaction of 2-propanol, but in absence of air, they got saturated.

In Fig. 7 the activity registered after 10 min of time on stream versus the calcination temperature of the catalysts, is shown. The crystalline phases detected by XRD at the different temperatures are marked. The best dehydrogenation activity was achieved when the precursor was

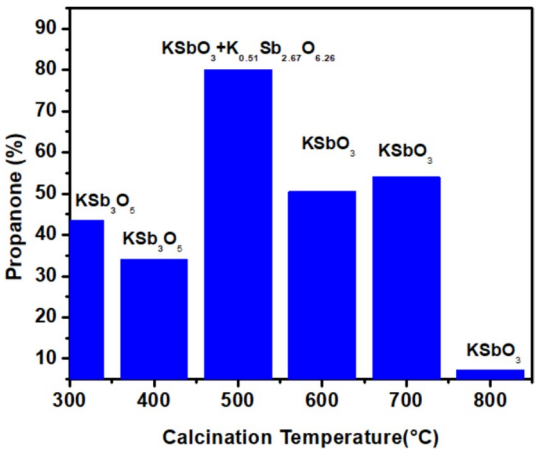

Fig. 7 Variation of the activity after 10 min at 200 °C under reaction stream in the presence of N_2 as the carrier gas as a function of the catalyst calcination temperature

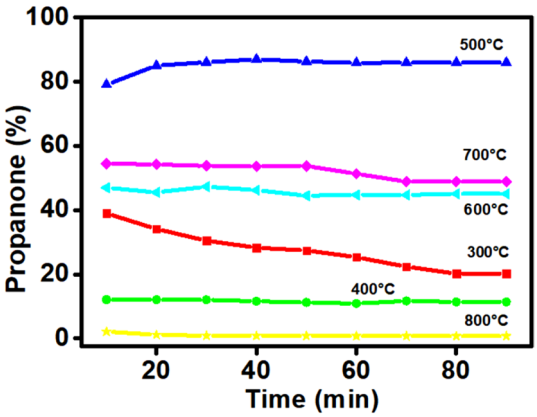

Fig. 8 Catalytic activity in the presence of air at 200 °C versus time on stream for catalysts at different calcination temperatures

calcined at 500 °C. At this temperature, two crystalline phases were detected, $KSbO_3$ as preponderant phase along with $K_{0.51}Sb_{2.67}O_{6.26}$ as secondary phase. According to the XRD characterization, starting from 500 °C the Sb exists as Sb(V), as main oxidation state. The highest catalytic activity registered for the sample calcined at 500 °C is likely due to the best compromise between Sb oxidation state (V), specific surface area and likely exposed basic sites as well as to the proper crystallite size of the $KSbO_3$ phase (see Table 2). The decreased surface and crystallite growth occurring by increasing the calcination temperature above 500 °C are likely responsible of the declined activity. This behaviour confirmed the occurrence of a dehydrogenation reaction involving the strong basic sites typical of KSbxOy oxides [39].

4.2 Catalytic Activity Under Air

The catalytic activity was also evaluated in the presence of air, the trend of propanone yield (%) versus time is displayed in Fig. 8 for catalysts calcined at different temperatures. An almost stable conversion was attained during all the reaction time differently from what observed in presence of N_2 (see Fig. 6). This finding suggests that the alcohol acts as the reducing agent and the oxygen present in the air is able to regenerate the Sb(V) active sites. The best conversion (~ 85%) was achieved with the sample calcined at 500 °C, while samples treated at T < 500 °C were less active, likely due to the presence of Sb(III) species and according to a poor basicity due to the presence of undecomposed organic matter. On the other hand, by increasing the calcination temperature up to 600–700 °C the 2-propanol conversion decreased with respect to the sample calcined at 500 °C, although at such high temperatures the crystalline phase present is always $KSbO_3$ containing Sb(V) active species. However, in spite of the favoured Sb oxidation state, at high calcination temperature a decrease of the specific surface area and likely of the exposed basic sites along with an increase of crystallite size occurs, causing a decreased activity, especially for the sample calcined at 800 °C that shows the worse conversion. Except for the sample calcined at 300 °C, a stable conversion over time was registered for the other samples, likely due to the achievement of stable crystalline phases with stable crystallite size. Independently on the calcination temperature, the 2-propanol is converted to 2-propanone confirming the active roles of basic and redox sites in the reaction.

5 Conclusions

From the results the following conclusions might be drawn:

- Calcination of potassium-antimony tartrate trihydrate $K(SbO)C_4H_4O_6.3H_2O$ in the range of temperature 300–800 °C produced KSbxOy mixed oxides with different crystalline phases, KSb_3O_5 prevailed below 500 °C, while $KSbO_3$ was formed at T ≥ 500 °C.
- The highest catalytic activity registered for the sample calcined at 500 °C is likely due to the best compromise between Sb oxidation state (V), specific surface area and likely amount of exposed basic sites as well as proper crystallite size of the $KSbO_3$ phase.
- The conversion of 2-propanol over KSbxOy mixed oxides produced 2-propanone with selectivity close to 100%, independently on the calcination temperature and atmosphere of the reaction, N_2 or air, suggesting that the active role in the reaction is played by the basic sites and as well by the presence of Sb(V)/Sb (III) redox couple.

- Under N_2 the activity reached the maximum after 10 min, but rapidly decreased with time on stream and almost declined after 1 h. After regeneration of the catalysts under air flow at 200 °C, the initial activity was gained.
- The presence of air in the reaction mixture favoured the re-oxidation of Sb(III) to the active Sb(V) ions, guaranteeing the regeneration of the redox couple.
- Based on the preliminary catalytic properties of KSbxOy mixed oxides discovered in the present study, additional investigations are in progress to assess their activity in other reactions, as the oxidation of long-chain alcohols.

Acknowledgements The Mohammed V University Project No. SCH 14/09 is acknowledged for financial support and the authors are grateful to CNRST for kindly providing necessary equipment to carry out experiments. L. F. Liotta has carried part of this research in the field of the COST Action 18224 "Green Chemical Engineering Network towards upscaling sustainable processes" and part in the field of the Italian PON MIUR "Energy for TARANTO" (Proposal Code ARS01_00637).

Compliance with Ethical Standards

Conflict of interest The authors declare that they have no conflict of interest.

References

1. Chin HS, Cheong KY, Razak KA (2010) Review on oxides of antimony nanoparticles: synthesis, properties, and applications. J Mater Sci 45(22):5993–6008. https://doi.org/10.1007/s10853-010-4849-x
2. Nieto JML, Solsona B (2018) 5.1 Principles of catalyst choice for selective oxidation reactions and historical aspects. J Metal Oxides in Heterog Catal. https://doi.org/10.1016/B978-0-12-811631-9.00009-0
3. Li B-L, Hu H-C, Mo L-P, Zhang Z-H (2014) Nano CoFe 2 O 4 supported antimony (III) as an efficient and recyclable catalyst for one-pot three-component synthesis of multisubstituted pyrroles. RSC Adv 4(25):12929–12943. https://doi.org/10.1039/C3RA47855F
4. Guan J, Wu S, Jia M, Huang J, Jing S, Xu H, Wang Z, Zhu W, Xing H, Wang H (2007) Effect of antimony doping on the catalytic behavior of Mo–V–Te–P mixed oxide catalysts in oxidation of isobutane. Catal Commun 8(8):1219–1223. https://doi.org/10.1016/j.catcom.2006.11.009
5. Miki J, Osada Y, Tachibana Y, Shikada T (1994) Oxidation of toluene to benzoic acid over modified V2O5-TiO2 catalyst with SeO2, TeO2 and Sb2O3. Catal Lett 30(1):263–268. https://doi.org/10.1007/BF00813692
6. Berry FJ (1998) Tin–antimony oxide oxidation catalysts. Hyperfine Interact 111(1–4):35–37. https://doi.org/10.1023/A:1012616625473
7. Spengler J, Anderle F, Bosch E, Grasselli R, Pillep B, Behrens P, Lapina O, Shubin A, Eberle H-J, Knözinger H (2001) Antimony oxide-modified vanadia-based catalysts physical characterization and catalytic properties. J Phys Chem B 105(44):10772–10783. https://doi.org/10.1021/jp012228u
8. Chang J-S, Hong D-Y, Vislovskiy VP, Park S-E (2007) An overview on the dehydrogenation of alkylbenzenes with carbon dioxide over supported vanadium-antimony oxide catalysts. Catal Surv Asia 11(1–2):59–69. https://doi.org/10.1007/s10563-007-9021-5
9. Burri A, Jiang N, Ji M, Park S-E, Khalid Y (2013) Oxidative dehydrogenation of ethylbenzene to styrene with CO2 Over V2O5–Sb2O5–CeO2/TiO2–ZrO2 Catalysts. Top Catal 56(18):1724–1730. https://doi.org/10.1007/s11244-013-0108-0
10. Stelzer J, Caro J, Fait M (2005) Oxidative dehydrogenation of propane on TiO2 supported antimony oxide/vanadia catalysts. Catal Commun 6(1):1–5. https://doi.org/10.1016/j.catcom.2004.10.001
11. Tan L, He M, Tang A, Chen J (2017) Preparation and enhanced catalytic hydrogenation activity of Sb/Palygorskite (PAL) nanoparticles. Nanoscale Res Lett 12(1):460. https://doi.org/10.1186/s11671-017-2220-8
12. Mao D, Xia J, Zhang B, Lu G (2010) Highly efficient synthesis of dimethyl ether from syngas over the admixed catalyst of CuO–ZnO–Al2O3 and antimony oxide modified HZSM-5 zeolite. Energy Convers Manage 51(6):1134–1139. https://doi.org/10.1016/j.enconman.2009.12.022
13. Liu G, Bonakdarpour A, Wang X, Bi X, Wilkinson DP (2019) Antimony-doped tin oxide nanofibers as catalyst support structures for the methanol oxidation reaction in direct methanol fuel cells. Electrocatalysis 10(3):262–271. https://doi.org/10.1007/s12678-019-00524-7
14. Xu J, Li Q, Hansen MK, Christensen E, García ALT, Liu G, Wang X, Bjerrum NJ (2012) Antimony doped tin oxides and their composites with tin pyrophosphates as catalyst supports for oxygen evolution reaction in proton exchange membrane water electrolysis. Int J Hydrog Energy 37(24):18629–18640. https://doi.org/10.1016/j.ijhydene.2012.09.156
15. Akbari A, Alavi S (2015) The effect of cesium and antimony promoters on the performance of Ti-phosphate-supported vanadium (V) oxide catalysts in selective oxidation of o-xylene to phthalic anhydride. J Chem Eng Res Design 102:286–296. https://doi.org/10.1016/j.cherd.2015.06.030
16. Park D-W, Park B-K, Park D-K, Woo H-C (2002) Vanadium-antimony mixed oxide catalysts for the selective oxidation of H2S containing excess water and ammonia. Appl Catal A 223(1):215–224. https://doi.org/10.1016/S0926-860X(01)00760-8
17. Guerrero-Pérez MO, Fierro JLG, Bañares MA (2006) Effect of synthesis method on stabilized nano-scaled Sb–V–O catalysts for the ammoxidation of propane to acrylonitrile. Top Catal 41(1):43–53. https://doi.org/10.1007/s11244-006-0093-7
18. Ballarini N, Cavani F, Giunchi C, Masetti S, Trifirò F, Ghisletti D, Cornaro U, Catani R (2001) Rutile-type Cr/Sb mixed oxides as heterogeneous catalysts for the ammoxidation of propane to acrylonitrile. Top Catal 15(2):111–119. https://doi.org/10.1023/A:1016666202748
19. Derouane-Abd Hamid SB, Centi G, Pal P, Derouane EG (2001) Site isolation and cooperation effects in the ammoxidation of propane with VSbO and Ga/H-ZSM-5 catalysts. Top Catal 15(2):161–168. https://doi.org/10.1023/A:1016652617893
20. Li L, Chai S-H, Binder A, Brown S, Veith GM, Dai S (2014) Catalytic CO oxidation over gold nanoparticles: support modification by monolayer- and submonolayer-dispersed Sb2O3. Catal Lett 144(5):912–919. https://doi.org/10.1007/s10562-014-1239-z
21. Wang X, Liu Y, Yao W, Wu Z (2019) Boosting the low-temperature activity and sulfur tolerance of CeZr2Ox catalysts by antimony addition for the selective catalytic reduction of NO with ammonia. J Colloid Interface Sci 546:152–162. https://doi.org/10.1016/j.jcis.2019.03.031
22. Phil HH, Reddy MP, Kumar PA, Ju LK, Hyo JS (2008) SO2 resistant antimony promoted V2O5/TiO2 catalyst for NH3-SCR of NOx at low temperatures. Appl Catal B 78(3–4):301–308. https://doi.org/10.1016/j.apcatb.2007.09.012

23. Du X, Gao X, Fu Y, Gao F, Luo Z, Cen K (2012) The co-effect of Sb and Nb on the SCR performance of the V2O5/TiO2 catalyst. J Colloid Interface Sci 368(1):406–412. https://doi.org/10.1016/j.jcis.2011.11.026
24. Udalova O, Shashkin D, Shibanova M, Krylov O (2005) Action of Co-Mo-Bi-Fe-Sb-K catalysts in the partial oxidation of propylene to acrolein: 1. The composition dependence of activity and selectivity. Kinet Catal 46(4):535–544. https://doi.org/10.1007/s10975-005-0106-8
25. Pang K, Kotek R, Tonelli A (2006) Review of conventional and novel polymerization processes for polyesters. Prog Polym Sci 31(11):1009–1037. https://doi.org/10.1016/j.progpolymsci.2006.08.008
26. Xue H, Lin X, Chen Q, Qian Q, Lin S, Zhang X, Yang D-P, Xiao L (2018) S-doped Sb(2)O(3) nanocrystal: an efficient visible-light catalyst for organic degradation. Nanoscale Res Lett 13(1):114–114. https://doi.org/10.1186/s11671-018-2522-5
27. Hu W, Zhang Y, Huang Y, Wang J, Gao J, Xu J (2015) Selective esterification of glycerol with acetic acid to diacetin using antimony pentoxide as reusable catalyst. J Energy Chem 24(5):632–636. https://doi.org/10.1016/j.jechem.2015.08.001
28. Reddy JR, Ravi G, Suresh P, Veldurthi NK, Velchuri R, Vithal M (2014) Antimony potassium tartrate. J Therm Anal Calorim 115(2):1321–1327. https://doi.org/10.1007/s10973-013-3502-8
29. Park J, Kim DH, Park SJ, Tg L, Im M, Kim JS, Nahm S (2016) Effects of K2O evaporation on the structural properties of KSbO3 compounds. J Am Ceram Soc 99(7):2229–2232. https://doi.org/10.1111/jace.14330
30. Merline GKP, Chitra M, Krishnan P (2015) Investigation on the crystal growth and characterization of an organometallic non-linear optical crystal-antimony potassium tartrate. Optik 126(24):5339–5341. https://doi.org/10.1016/j.ijleo.2015.09.247
31. Barbosa VT, de Menezes JB, Santos JCC, de Assisastos ML, Araújo-Júnior JX, do Nascimento TG, Basílio-Júnior ID, Grillo LAM, Dornelas CB (2019) Characterization and stability of the antimony-quercetin complex. Adv Pharm Bull 9(3):432. https://doi.org/10.15171/apb.2019.051
32. Kim Y-K, Hao LF, Park JI, Miyawaki J, Mochida I, Yoon SH (2012) Catalytic activity and activation mechanism of potassium carbonate supported on perovskite oxide for coal char combustion. Fuel 94:516–522. https://doi.org/10.1016/j.fuel.2011.10.017
33. Reddy JR, Veldurthi NK, Palla S, Ravi G, Guje R, Vithal M (2014) Facile ion-exchange synthesis of visible light active Sn-doped defect pyrochlore K0. 51Sb2. 67O6. 26 and study of its photocatalytic activity. J Chem Technol Biotechnol 89(12):1833–1841. https://doi.org/10.1002/jctb.4264
34. Jasińska E, Krzyżyńska B, Kozłowski M (2008) Activated carbon modified with different chemical agents as a catalyst in the dehydration and dehydrogenation of isopropanol. Catal Lett 125(1–2):145–153. https://doi.org/10.1007/s10562-008-9536-z
35. Bautista FM, Campelo JM, Garcia A, Luna D, Marinas JM, Romero AA, Urbano MR (1995) Conversion of 2-propanol over chromium aluminum orthophosphates. Catal Lett 35(1–2):143–154. https://doi.org/10.1007/BF00807012
36. Ciriminna R, Pandarus V, Beland F, Xu Y-J, Pagliaro M (2015) Heterogeneously catalyzed alcohol oxidation for the fine chemical industry. Organic Process Res Dev 19(11):1554–1558. https://doi.org/10.1021/acs.oprd.5b00204
37. Lercher JA, Jentys A, Brait A (2008) Catalytic test reactions for probing the acidity and basicity of zeolites. Acidity and Basicity. Springer, Berlin. https://doi.org/10.1007/3829_2007_017
38. Ali AH, Zaera F (2002) Kinetic study on the selective catalytic oxidation of 2-propanol to acetone over nickel foils. J Mol Catal A: Chem 177(2):215–235. https://doi.org/10.1016/S1381-1169(01)00223-0
39. Fraile JM, García N, Mayoral JA, Pires E, Roldán L (2009) The influence of alkaline metals on the strong basicity of Mg–Al mixed oxides: the case of transesterification reactions. Appl Catal A 364(1–2):87–94. https://doi.org/10.1016/j.apcata.2009.05.031